ACS APPLIED MATERIALS & INTERFACES

www.acsami.org

Research Article

Extrapolated Defect Transition Level in Two-Dimensional Materials: The Case of Charged Native Point Defects in Monolayer Hexagonal Boron Nitride

Xuefei Liu, Zhibin Gao, Vei Wang, Zijiang Luo, Bing Lv, Zhao Ding,* and Zhaofu Zhang*

Cite This: *ACS Appl. Mater. Interfaces* 2020, 12, 17055−17061

Read Online

ACCESS | Metrics & More | Article Recommendations | Supporting Information

ABSTRACT: Defect formation energy as well as the charge transition level (CTL) plays a vital role in understanding the underlying mechanism of the effect of defects on material properties. However, the accurate calculation of charged defects, especially for two-dimensional materials, is still a challenging topic. In this paper, we proposed a simplified scheme to rescale the CTLs from the semilocal to the hybrid functional level, which is time-saving during the charged defect calculations. Based on this method, we systematically calculated the formation energy of four kinds of intrinsic point defects in two-dimensional hexagonal boron nitride (2D h-BN) by uniformly scaling the supercells by which we found a time-saving method to obtain the "special vacuum size" (Komsa, H.-P.; Berseneva, N.; Krasheninnikov, A. V.; Nieminen, R. M. *Phys. Rev. X*, **2014**, *4*, 031044). Native defects including nitrogen vacancy (V_N), boron vacancy (V_B), nitrogen atom anti-sited on boron position (N_B), and boron atom anti-sited on nitrogen position (B_N) were calculated. The reliability of our scheme was verified by taking V_N as a probe to conduct the hybrid functional calculation, and the rescaled CTL is within the acceptable error range with the pure HSE results. Based on the results of CTLs, all the native point defects in the h-BN monolayer act as hole or electron trap centers under certain conditions and would suppress the p- or n-type electrical conduction of h-BN-based devices. Our rescale method is also suitable for other materials for defect charge transition level calculations.

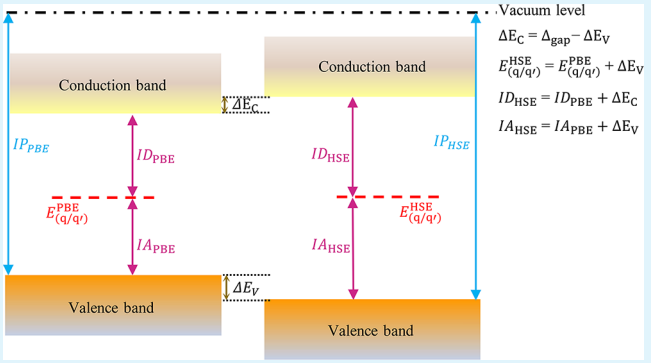

KEYWORDS: *defect formation energy, charge transition level, native point defects, two-dimensional materials, h-BN monolayer*

Downloaded via NATL UNIV OF SINGAPORE on July 8, 2021 at 06:11:22 (UTC).
See https://pubs.acs.org/sharingguidelines for options on how to legitimately share published articles.

1. INTRODUCTION

The intentional control for electronic conductivity can be achieved by engineering the native defects or impurities, and typical cases for the former include vacancies, substitutions, and interstitials.[1] Full comprehension of semiconductor defects, especially charged defect physics, is desired owing to its decisive role in determining material properties such as optical, mechanical, electrical, and transport properties and thus the corresponding applications.[2−6] It is rather difficult to directly investigate the charged defects in materials by experiments at the atomic level. Instead, first-principle calculations play vital roles in understanding defect properties and providing theoretical guidance in improving device performance, efficiency, and reliability.[7−9]

As widely reviewed, charged defects calculation for 3D (or bulk) materials is full of challenges, and one of the reasons is due to the spurious long-range Coulomb interactions between the periodic images and the neutralizing background charges, which are introduced to avoid the divergence during the self-consistent calculation. These, in turn, would influence the accuracy of the calculated defect formation energy and charge transition level (CTL).[7,8] As for the 2D materials, i.e., slab models, more obstacles emerge. The in-homogeneous dielectric environments normal to the vacuum slab in 2D slab models would cause further troubles to precisely evaluate defect properties.[3,10−14] Komsa and Pasquarello first developed a finite-size supercell correction scheme for removing spurious electrostatic interactions of charged defects for surfaces and interfaces,[10] which could obtain the correct defect formation energy even for a relatively small supercell. They also stressed that the supercells need to be enlarged uniformly in three directions to guarantee the convergence of defect formation energy.[10] The authors extended this scheme for 2D materials by choosing the dielectric constant profile to follow the charge density distribution of the system[11] where they, for the first time, proposed the so-called "special vacuum size" (SVS)

Received: December 27, 2019
Accepted: March 13, 2020
Published: March 13, 2020

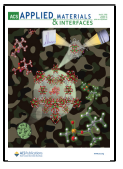

ACS Publications

© 2020 American Chemical Society

method to precisely calculate the defect formation energy of 2D materials. In detail, they concluded that, for a given supercell, the defect formation energy varies with the different vacuum thickness. That is, the defect formation energy can be either lower or higher than the correct value under different vacuum sizes, indicating that there exists a vacuum size, i.e., SVS, to guarantee the exact formation energy without any correction or extrapolation. However, it is tedious to obtain the SVS because one needs to gain the correct defect formation energy in advance and then scales the vacuum sizes gradually for different supercell sizes. While in our study, we find that the SVS could be uniformly scaled as well, which counts because we can vary the vacuum size in a relatively small supercell to find a corresponding SVS and then scale the vacuum size with a fixed ratio to obtain an SVS for a much larger supercell to conduct new calculations. Recently, Freysoldt and Neugebauer reported a method to calculate the formation energy of charged defects at surfaces, interfaces, or two-dimensional materials[14] where they applied periodic boundary conditions to the periodic slab case and open boundary conditions for the surface or 2D case in the same scheme, indicating that one does not need to resort to the finite-size extrapolation to obtain the isolated energy. Up to now, Freysoldt's method is one of the time-saving and flexible schemes on the corrections of 2D charged defect calculations. Thus, we adopted this method to correct formation energy and compare the results with those obtained by the extrapolated method.

Another challenge is that the density functional theory using the local density approximation (LDA) or the generalized gradient approximation (GGA) often severely underestimates the band gap. As a result, the accuracy of defect formation energies and CTLs are significantly impacted.[7,8] A hybrid functional such as Heyd−Scuseria−Ernzerhof (HSE[15]) would overcome the band gap underestimation problem, but often the time consumption involved is prohibitive, especially for a large supercell, which is usually used to mimic the low defect concentration of realistic materials. It is noted that, despite the band gap narrowing by the semilocal GGA functional, the calculated formation energy is similar to that by the HSE functional.[16,17] Thus, the derived charge transition level from the Perdew−Burke−Ernzerhof (PBE) functional can be rescaled to the HSE scale,[16,17] despite more or less shortcomings.[18] Nieminen et al. compared the PBE CTLs with those calculated under the HSE functional by normalizing the band gaps,[16] while in refs 17 and 19, the authors simply corrected the CTLs by adding half (all) of the bulk band gap difference between HSE and PBE functionals to the PBE derived CTLs. However, note that the HSE calculation does not necessarily open the band gap by repulsing conduction band minimum (CBM) and valence band maximum (VBM) identically.[20] In this paper, we propose a new scaling scheme and consider the differences of the VBM position (i.e., the ionic potentials, IP) and band gap values under two different functionals (i.e., PBE and HSE functionals) so that the formation energy can be calculated more reasonably and reliably.

In this work, we apply our calculation scheme to the charged native defects in a hexagonal boron nitride (h-BN) monolayer, which has superior optical, electrical, and mechanical properties.[21,22] Furthermore, single-photon emission has been observed in the h-BN monolayer at room temperature, which is promising for quantum information devices. Many defect configurations (i.e., color centers) are proposed for the possible single-photon emitters.[23−29] Despite the fact that many works on defect calculations of h-BN have been reported during the past decades,[14,17,19,30−36] the authors either did not calculate charged defects in h-BN or did but not corrected the defect formation energy with a reasonable 2D correction method. Besides, the charged anti-sited defects with proper correction were not considered either. Van de Walle et al. reported the charged native defects and CTLs of h-BN, but they are in the 3D structure model, which will inevitably more or less vary from the monolayer 2D case.[37,38] In this study, we systematically investigated the atomic structures, defect formation energies, and CTLs of native point defects in h-BN, including nitrogen vacancy (V_N), boron vacancy (V_B), nitrogen atom anti-sited on boron position (N_B), and boron atom anti-sited on nitrogen position (B_N) in multiple charge states with 2D defect correction as well as extrapolating methods. The extracted defect charge transition levels by rescaling correspond well with that by the practical HSE functional, indicating that our proposed rescaling methodology is reasonable. In principle, the proposed CTL rescale method can also be applicable for other 2D or 3D defect charge transition level calculations.

2. COMPUTATION METHODS

The calculations were conducted based on spin-polarized density functional theory with GGA-PBE functional[39] and projector augmented wave (PAW) potential,[40] as implemented in the VASP code.[41] An energy cutoff of 400 eV was used. A reciprocal space was sampled with 5 × 3 × 1, 3 × 2 × 1, 2 × 1 × 1, and 1 × 1 × 1 Monkhorst−Pack k-point mesh for the 3 × 3 × 3 to 6 × 6 × 6 supercells, respectively. All atoms were relaxed until the Hellman−Feynman force on each atom was less than 0.01 eV/Å and the energy convergence criterion was 10^{-6} eV. To validate our proposed rescale scheme, charged V_N supercells were calculated by the HSE06 functional and compared with the PBE derived data.

During the calculations, we redefined the lattice of the h-BN primitive cell into an orthogonal form using VASPKIT, a pre- and post-processing program for the VASP code,[42] as shown in Figure 1,

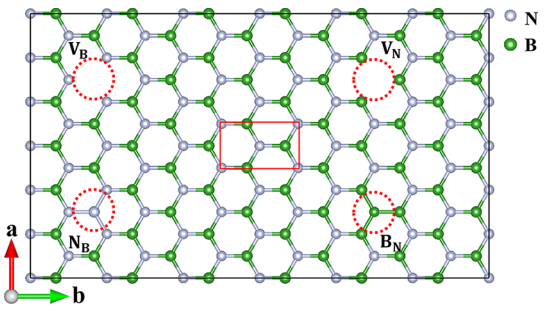

Figure 1. Supercell (6 × 6, with 144 atoms) with the minimum repeat unit of h-BN highlighted by the red rectangle. The sketch maps of four intrinsic defects are marked by red dotted circles.

to take advantage of the correction scheme proposed by Freysoldt, Neugebauer, and Van de Walle (FNV).[14] The optimized unit cell lattice is a = 2.51 Å, b = 4.35 Å, and with an SVS of 7.50 Å. When point defects were introduced into the h-BN host, we calculated 3 × 3 × 3, 4 × 4 × 4, 5 × 5 × 5, and 6 × 6 × 6 supercells with linearly scaled vacuum thickness, implying that all the supercells were scaled uniformly in both the x-y plane and the z direction by which the formation energies would converge linearly to a finite value.[11] Again, it is of particular importance and necessary to uniformly enlarge the vacuum size to maintain the converged defect transition level.

https://dx.doi.org/10.1021/acsami.9b23431
ACS Appl. Mater. Interfaces 2020, 12, 17055−17061

The formation energy of an isolated charged defect in the 2D h-BN monolayer is defined as

$$E^{f}_{\infty}[X^{q}] = E^{f}_{finite}[X^{q}] + E_{correct} \quad (1)$$

where $E^{f}_{\infty}[X^{q}]$ and $E^{f}_{finite}[X^{q}]$ are the defect formation energies of the infinite and finite h-BN supercells containing a defect in charge state q, respectively, and $E_{correct}$ is a correction term by the FNV method[14] or extrapolating[11] and is different from the 3D defect case. Specially, $E_{correct}$ can be obtained by uniformly extending the supercells in the case of extrapolating, which is not necessary in the 3D case. In contrast, if $E_{correct}$ is obtained by posteriori correction with FNV method, then the Poisson equation should be solved by particularly considering the distribution of the dielectric function in the vacuum direction of the model. The very detailed description about the charged defect formation energy, especially the correction term, is in the Supporting Information.

The charge transition level (CTL) is determined by[7,8]

$$E_{(q/q')} = \frac{E^{f}(q; E_{f} = 0) - E^{f}(q'; E_{f} = 0)}{q - q'} \quad (2)$$

where $E^{f}(q; E_{f} = 0)$ and $E^{f}(q'; E_{f} = 0)$ represent the formation energies for the states of charge q and q', respectively. The energy difference between the transition level and band edges determines the donor/acceptor ionization energy, denoted as

$$ID = CBM - E_{(q/q')} \quad (3)$$

and

$$IA = E_{(q/q')} - VBM \quad (4)$$

respectively, which can be used to directly judge the depth of a certain defect energy level.

3. RESULTS AND DISCUSSIONS

First, the FNV method[14] was used to calculate the $E_{correct}$ term in eq 1 in which the method of the alignment term $\Delta V_{q-0}/m$ in eq S5 is required to well converge to a constant in the region far from the defect (i.e., in the vacuum region), as seen in Figure 2 (blue line). For the sake of simplicity, only the alignment plot of the charged boron vacancy defect (V_B^{+1} and V_B^{-1}) is illustrated as an example.

Then, we calculated the formation energies of different defects in all supercell sizes, and the results are shown in Figure 3. It is observed that all the formation energies vary linearly with the inversed scale sizes, similar to those in refs 10, 11, and 43, owing to the uniformly cell-enlarged method. Besides,

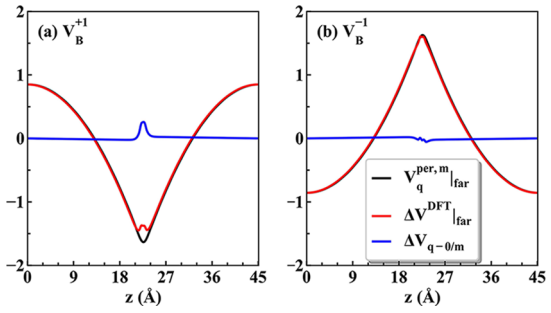

Figure 2. Alignment of the model potentials of (a) V_B^{+1} and (b) V_B^{-1} in a 6 × 6 × 6 supercell. All potentials are averaged over the x-y plane. Red line, defect-induced change in the DFT electrostatic potentials without corrections; black line, the model potentials from the FNV scheme;[14] and blue line, the alignment between the model potentials and the DFT difference (see the Supporting Information) potentials, represented as ΔV^{DFT}_{far}.

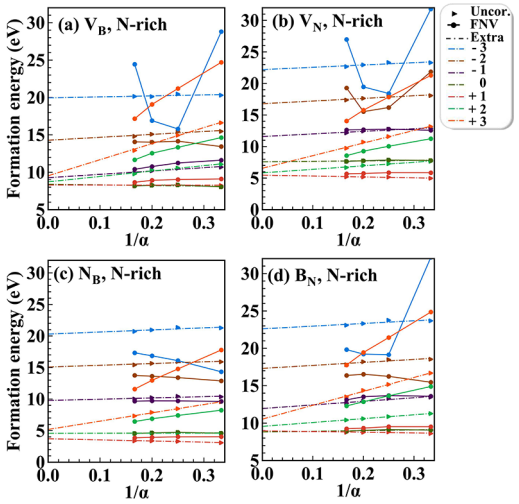

Figure 3. Formation energies under different charge states for native point defects under N-rich limitation in h-BN monolayers as a function of the inversed scale times ($1/\alpha$, α = 3,4,5, and 6) of supercell size for the (a) V_B, (b) V_N, (c) N_B, and (d) B_N defect system, respectively. Circle-solid lines represent the corrected formation energies with the FNV method, the triangle represents raw data without corrections, and dotted lines represent extrapolated formation energy to an infinite supercell case. The different charge states are labeled as various colors.

almost all the formation energies are converged well. That is to say, for a given defect type under a certain charge state, the formation energies barely vary among different supercell sizes. These well-converged formation energies imply that all the vacuum sizes in different supercells are the exact (or very close to the) SVSs,[11] considering that all the vacuum sizes are obtained by uniformly enlarged supercells. Thus, we deduce that the SVS can be uniformly enlarged as well. To further verify this speculation, we also uniformly scale and obtain the SVSs of all supercells (with different shapes) in ref 11 based on the normalized vacuum thickness of the 10 × 10 supercell. The derived SVSs (Table 1, last row) are close to those reported in ref 11 with an average error of less than 2.8%. This indicates that the scalability of SVS is reliable, which has not been proposed by previous reports. The finding manifests that we can choose a relatively smaller supercell to test the SVS by fixing the x-y size and varying the z (vacuum) thickness before starting a calculation with a larger supercell; thus, it is time-saving.

Compared with the extrapolated values (the dotted line at $1/\alpha = 0$), which is the most accurate method up till now, one can find that only the results of ±1 and some ±2 charge states are well corrected by the FNV method. This implies that the FNV method would work better in lower charge states than higher charge cases, similar to those reported in refs 14 and 43. However, it is still acceptable considering the general higher formation energies at higher charge states.

Based on the similar defect formation energies between the two functionals,[16] we propose that the calculated CTL by the PBE functional can be rescaled to the HSE functional scale using the scheme plotted in Figure 4. The band gap and ionic potential (energy difference between vacuum and VBM) of the h-BN unit cell were first calculated by PBE and HSE functionals to obtain the band edge offsets (ΔE_V and ΔE_C), and our calculated gap and IP values agree very well with previous reports.[44] As illustrated, the band offsets differ

https://dx.doi.org/10.1021/acsami.9b23431
ACS Appl. Mater. Interfaces 2020, 12, 17055−17061

Table 1. SVS (in Å) for Different Lateral Supercell Sizes Based on the Orthogonal Unit Cell (Labeled as OC, Shown in Figure 1) or the Standard h-BN Primitive Cell (from Ref 11, Labeled as PC)[a]

lattice size		3 × 3		4 × 4		5 × 5		6 × 6
uniformly scaled SVS in this paper (OC) (Å)		22.5		30		37.5		45
lattice size	4 × 4	5 × 5	6 × 6	7 × 7	8 × 8	9 × 9	10 × 10	
SVS in ref 11 (PC) (Å)	16.35	20.82	25.44	30.11	34.79	39.43	43.99	
uniformly scaled SVS using data in ref 11 (Å)	17.59	21.99	26.39	30.79	35.19	39.59	43.99	

[a]The uniformly scaled SVSs of different supercells are also shown.

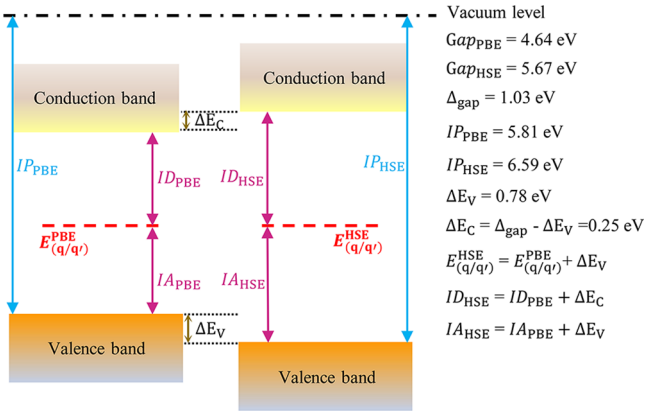

Figure 4. Schematic of the rescaling scheme used in this paper. The charge transition level calculated within the semilocal PBE and the hybrid HSE functional are marked as $E^{PBE}_{(q/q')}$ and $E^{HSE}_{(q/q')}$, respectively, aligned to the vacuum level. ΔE_V and ΔE_C are shifts of the VBM and CBM between the two functionals, respectively. IP represents the ionic potential, i.e., energy difference between the vacuum level and VBM, while ID and IA represent the donor and acceptor ionization energies (eqs 3 and 4), respectively. The rescaled HSE transition level is obtained by adding ΔE_V to PBE calculation ($E^{PBE}_{(q/q')}$).

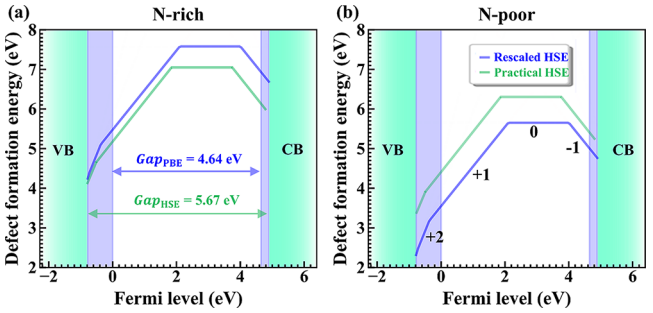

Figure 5. Calculated formation energies of an isolated V_N in the h-BN monolayer in different charge states as a function of the Fermi level range from VBM to CBM for (a) N-rich and for (b) N-poor limitation conditions. The rescaled and practical HSE results are labeled as the blue and green lines, respectively.

distinctly from each other (ΔE_V is 0.78 eV while ΔE_C is 0.25 eV). So, the previously proposed CTL rescaling methods by roughly adding half (all) of Δ_{gap}[17,19] are not so robust. In our work, the HSE-scale CTL is obtained by adding the ΔE_V to the PBE-scale CTL, i.e., $E^{HSE}_{(q/q')} = E^{PBE}_{(q/q')} + \Delta E_V$. That is to say, the differences between both the band gap value and band edge positions were considered in our scheme. Furthermore, the donor (acceptor) ionization energies were rescaled as well, i.e., $ID_{HSE} = ID_{PBE} + \Delta E_C$ ($IA_{HSE} = IA_{PBE} + \Delta E_V$). So, all the calculations involved for the charged defect calculation are only PBE functional (rather than HSE) for supercells with different defect configurations or charge states as well as an HSE functional calculation for the pristine bulk material (only several atoms) to determine the band edge positions, which saves much time compared with the standard HSE defect calculation procedures. Based on the method described above, we will discuss the CTL of native point defects in h-BN. Additionally, to verify the reliability of our rescaled method, we took the V_N system as a benchmark check to conduct practical HSE calculations.

3.1. Discussions on V_N. After full relaxation, the B-B distances around V_N under a neutral or −1 charge state are decreased from 2.51 to 2.07 and 2.29 Å, respectively, owing to the electrostatic attraction between the boron atoms. The most stable charge states (MSCSs) for V_N defect are V_N^{-1}, V_N^{0}, V_N^{+1}, and V_N^{+2} when the Fermi energy is swept from VBM to CBM, as shown in Figure 5, in which both the rescaled and practical HSE CTL results are illustrated. Note that the HSE CTLs (both rescaled or practical) can be obtained just by referencing the HSE-calculated VBM as the zero points of the x axis. For instance, the rescaled $E^{HSE}_{(+2/+1)}$, $E^{HSE}_{(+1/0)}$, and $E^{HSE}_{(0/-1)}$ lie ∼0.4, ∼2.8, and ∼4.8 eV above the VBM, respectively, and their corresponding practical HSE CTLs are 0.2, 2.6, and 4.6 eV, respectively. All the CTLs in our rescaled results are overestimated only ∼0.2 eV within the error range mentioned in ref 18. Specially, the $E^{HSE}_{(+1/0)}$ (∼2.8 eV) is comparable to a value of ∼3.5 eV in ref 3 if we rescale our HSE level to the GW level with a similar process. The discrepancy here is mainly derived from the different band gaps of the HSE (5.7 eV) and GW (7.2 eV) method. Additionally, $E^{HSE}_{(0/-1)}$ (∼4.6 eV) also agrees with a value of 4.6 eV in ref 37 where a bulk phase of BN was calculated. The errors of formation energies are found to vary from 0.1 to 0.5 eV under different charge states within the same error range in ref 16, confirming that our rescaled results are reliable. To expediently judge the depth of donor or acceptor nature, the donor ionization energies (ID_{HSE}; eq 3) with the rescaled (practical) HSE method for $E^{HSE}_{(+2/+1)}$ and $E^{HSE}_{(+1/0)}$ are calculated to be 5.3 (5.5) and 2.8 (3.0) eV, respectively. Likewise, the acceptor ionization energy (IA_{HSE}; eq 4) for $E^{HSE}_{(0/-1)}$ is 4.8 (4.6) eV, indicating that all of the donors (acceptors) are deep and do not effectively contribute conductivity but expect to be recombination centers. Note that the formation energy of V_N in the whole electron chemical potential range under N-rich (or poor) limitation is high enough to hinder the defects to be introduced. However, with relative lower formation energy, V_N^{+2} in p-type h-BN under N-poor limitation may be non-negligible to affect the properties of h-BN.

3.2. Discussions on V_B. As shown in Figure 6, the MSCSs for V_B defect are V_B^{-1}, V_B^{0}, V_B^{+1}, and V_B^{+2} as well. The N-N distances around V_B in all charge states increase significantly, respect to that of pristine h-BN, i.e., from 2.51 to 2.65 Å, due to the Coulomb repulsion between nitrogen atoms around the

https://dx.doi.org/10.1021/acsami.9b23431
ACS Appl. Mater. Interfaces 2020, 12, 17055−17061

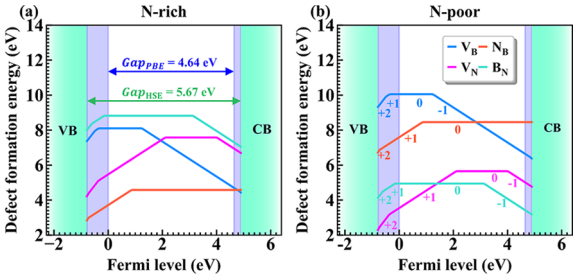

Figure 6. Calculated formation energies of the isolated native defects of V_B, V_N, N_B, and B_N in the h-BN monolayer for their stable charge states as a function of the Fermi level in (a) N-rich and (b) N-poor limitation conditions. The rescaled HSE CTLs can be obtained by referencing the zero-point of the x axial to the HSE VBM. The PBE and HSE gaps are labeled as blue and green colors, respectively.

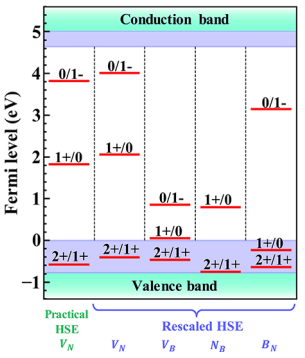

Figure 7. Stable charge states and CTLs of the isolated native defects of V_N, V_B, N_B, and B_N in the h-BN monolayer, and the PBE (HSE) conduction and valence band are labeled as blue (green) colors. The practical HSE CTLs are illustrated in the first column. By referencing HSE VBM to zero point, the CTLs can be rescaled from PBE to HSE values.

boron vacancy. The rescaled $E^{HSE}_{(+2/+1)}$, $E^{HSE}_{(+1/0)}$, and $E^{HSE}_{(0/-1)}$ levels lie ~0.3, ~0.8, and ~1.6 eV above the VBM, with their corresponding donor or acceptor ionization energy of 5.3, 4.8, and 1.6 eV, respectively. The $E^{HSE}_{(0/-1)}$ is close to that in ref 37 (1.48 eV). Clearly, V_B is both a deep donor and a deep acceptor, thus will not enable n- and p-type conductivity in h-BN monolayers. Furthermore, V_B is expected to barely exist under equilibrium growth conditions due to the high formation energy even in the N-rich ambient.

3.3. Discussions on N_B. By substituting a nitrogen atom with boron, the anti-sited N_B system shows MSCSs of 0, +1, and +2 (Figure 6). The neutral charge state N_B^0 is stable in a large range of electron chemical potential. $E^{HSE}_{(+2/+1)}$ is found near HSE VBM as well as $E^{HSE}_{(+1/0)}$ locates ~1.6 eV above VBM, and with an ID_{HSE} of ~4.1 eV, both show to be many deep donors, similar to those of bulk h-BN in ref 37. Thus, N_B hardly contributes electron carriers but acts as hole trap centers in the h-BN monolayer under nonequilibrium conditions.

3.4. Discussions on B_N. As shown in Figure 6, the rescaled $E^{HSE}_{(+2/+1)}$ and $E^{HSE}_{(+1/0)}$ for the B_N system are located at ~0.1 and ~0.5 eV, respectively, but with a rather large formation energy. The concentration of B_N in the h-BN monolayer is thus expected to be extremely low under thermodynamic equilibrium conditions, and it is an undesired donor for h-BN. In addition, $E^{HSE}_{(0/-1)}$ locates ~3.9 eV above VBM, acting as an electron trap center in an n-type doped h-BN monolayer.

The relative stability of four kinds of native point defects for the h-BN monolayer can be compared in Figure 6 as well. N_B^{+2}, N_B^{+1}, and N_B^0 states show the most stable defects when the Fermi level changes from VBM to about ~5.5 eV, while V_B^{-1} is found to be the most stable one after that. Additionally, the formation energy of N_B^{+2} at VBM is about ~2.9 eV and V_B^{-1} at CBM is 4.2 eV. The large formation energy means that the corresponding defect concentrations under N-rich limitation conditions are low under thermodynamic equilibrium conditions, although they can be generated artificially by atomic excitation techniques such as electron irradiation and atomic manipulation.[45] In contrast, in N-poor limitation conditions, V_N^{+2} and V_N^{+1} are found to be most stable when the Fermi level changes from VBM to ~2.2 eV, and after that, the MSCSs are B_N^0 and B_N^{-1} and the formation energy is about 3.0 eV for $B_N^{-1}$when the Fermi level is at the CBM. Thus, the concentration of B_N^{-1} is negligible in the N-poor limitation under equilibrium conditions.

3.5. Discussion on CTLs. The CTLs calculated by eq 2 are summarized in Figure 7 for a clear comparison between different native point defects. By referencing HSE VBM to zero point, the CTLs can be rescaled from PBE to HSE values. As seen in Figure 7, V_N and B_N show a much deep acceptor nature in the n-type doping h-BN monolayer. The only relative shallow singlet acceptor is V_B. All kinds of defects show a deep multidonor nature with rescaled HSE results. Thus, these levels are too high to be thermally ionized at device-operating temperatures. As a result, we expect that the unintentionally doped h-BN monolayer exhibiting either n- or p-type behavior cannot be attributed to the native defects.

4. CONCLUSIONS

In this paper, we proposed a simplified scheme to rescale the charge transition levels from the semilocal PBE to the hybrid HSE functional, which not only significantly improves the accuracy of the PBE CTL results but also saves much time during the calculations of charged defects. We also found that the special vacuum size in the 2D slab model is uniformly scalable as well as the scalability is supercell shape-independent, which provides a time-saving method to obtain the SVS for a larger supercell by testing it out with a smaller supercell. Based on our proposed scheme, we have systematically investigated the charged native point defects of V_N, V_B, N_B, and B_N in the h-BN monolayer, and the reliability of this rescaled method was verified by choosing the V_N system as a benchmark check to carry out authentic HSE calculations. The results show that the native point defects cannot be efficient dopants (electrons or holes) in a single-layer h-BN but act as recombination centers by which the electrical conductivity in h-BN monolayer-based electronic devices can be suppressed in the presence of the native defects.

■ ASSOCIATED CONTENT

Supporting Information

The Supporting Information is available free of charge at https://pubs.acs.org/doi/10.1021/acsami.9b23431.

The details for the correction of charged defect formation energy about 2D materials (PDF)

■ AUTHOR INFORMATION

Corresponding Authors

Zhao Ding − *College of Big data and Information Engineering, Guizhou University, Guiyang 550025, China; Semiconductor*

https://dx.doi.org/10.1021/acsami.9b23431
ACS Appl. Mater. Interfaces 2020, 12, 17055−17061

Power Device Reliability Engineering Center of Ministry of Education, Guiyang 550025, China; Email: zding@gzu.edu.cn

Zhaofu Zhang − *Department of Engineering, University of Cambridge, Cambridge CB2 1PZ, United Kingdom*; orcid.org/0000-0002-1406-1256; Email: zz389@cam.ac.uk

Authors

Xuefei Liu − *College of Big data and Information Engineering, Guizhou University, Guiyang 550025, China; Semiconductor Power Device Reliability Engineering Center of Ministry of Education, Guiyang 550025, China; Key Laboratory of Low Dimensional Condensed Matter Physics of Higher Educational Institution of Guizhou Province, Guizhou Normal University, Guiyang 550025, China*

Zhibin Gao − *Department of Physics, National University of Singapore, Singapore 117551, Republic of Singapore*; orcid.org/0000-0002-6843-381X

Vei Wang − *Department of Applied Physics, Xi'an University of Technology, Xi'an 710054, China*; orcid.org/0000-0002-9499-1823

Zijiang Luo − *Semiconductor Power Device Reliability Engineering Center of Ministry of Education, Guiyang 550025, China; College of Information, Guizhou Finance and Economics University, Guiyang 550025, China*

Bing Lv − *Key Laboratory of Low Dimensional Condensed Matter Physics of Higher Educational Institution of Guizhou Province, Guizhou Normal University, Guiyang 550025, China*

Complete contact information is available at: https://pubs.acs.org/10.1021/acsami.9b23431

Notes

The authors declare no competing financial interest.

■ ACKNOWLEDGMENTS

This work is supported by the National Natural Science Foundation of China (grant nos. 61564002 and 11664005), the Joint Foundation of Guizhou Normal University (grant no. 7341), the Scientific and Technological Cooperation Projects of Guizhou Province, China (grant no. [2013]7019), the Guizhou Normal University Innovation and Entrepreneurship Education Research Center Foundation (grant no. 0418010), and the Key laboratory of Low Dimensional Condensed Matter Physics of Higher Educational Institution of Guizhou Province (grant no. [2016]002). Z.G. acknowledges the financial support from MOE tier 1 funding of NUS Faculty of Science, Singapore (grant no. R-144-000-402-114). V.W. acknowledges the financial support of the Special Scientific Research Program of the Education Bureau of Shanxi Province, China (grant no. 15JK1531).

■ REFERENCES

(1) Wang, D.; Li, X.-B.; Han, D.; Tian, W. Q.; Sun, H.-B. Engineering Two-Dimensional Electronics by Semiconductor Defects. *Nano Today* **2017**, *16*, 30−45.

(2) Queisser, H. J.; Haller, E. E. Defects in Semiconductors: Some Fatal, Some Vital. *Science* **1998**, *281*, 945−950.

(3) Wu, F.; Galatas, A.; Sundararaman, R.; Rocca, D.; Ping, Y. First-Principles Engineering of Charged Defects for Two-Dimensional Quantum Technologies. *Phys. Rev. Mater.* **2017**, *1*, No. 071001.

(4) Liu, Y.; Gao, Z.; Tan, Y.; Chen, F. Enhancement of out-of-Plane Charge Transport in a Vertically Stacked Two-Dimensional Heterostructure Using Point Defects. *ACS Nano* **2018**, *12*, 10529−10536.

(5) Gerosa, M.; Gygi, F.; Govoni, M.; Galli, G. The Role of Defects and Excess Surface Charges at Finite Temperature for Optimizing Oxide Photoabsorbers. *Nat. Mater.* **2018**, *17*, 1122.

(6) Zheng, Y. J.; Chen, Y.; Huang, Y. L.; Gogoi, P. K.; Li, M.-Y.; Li, L.-J.; Trevisanutto, P. E.; Wang, Q.; Pennycook, S. J.; Wee, A. T. S.; Quek, S. Y. Point Defects and Localized Excitons in 2D WSe_2. *ACS Nano* **2019**, *13*, 6050−6059.

(7) Van de Walle, C. G.; Neugebauer, J. First-Principles Calculations for Defects and Impurities: Applications to III-Nitrides. *J. Appl. Phys.* **2004**, *95*, 3851−3879.

(8) Freysoldt, C.; Grabowski, B.; Hickel, T.; Neugebauer, J.; Kresse, G.; Janotti, A.; Van de Walle, C. G. First-Principles Calculations for Point Defects in Solids. *Rev. Mod. Phys.* **2014**, *86*, 253.

(9) Oba, F.; Kumagai, Y. Design and Exploration of Semiconductors from First Principles: A Review of Recent Advances. *Appl. Phys. Express* **2018**, *11*, No. 060101.

(10) Komsa, H.-P.; Pasquarello, A. Finite-Size Supercell Correction for Charged Defects at Surfaces and Interfaces. *Phys. Rev. Lett.* **2013**, *110*, No. 095505.

(11) Komsa, H.-P.; Berseneva, N.; Krasheninnikov, A. V.; Nieminen, R. M. Charged Point Defects in the Flatland: Accurate Formation Energy Calculations in Two-Dimensional Materials. *Phys. Rev. X* **2014**, *4*, No. 031044.

(12) Wang, D.; Han, D.; Li, X.-B.; Xie, S.-Y.; Chen, N.-K.; Tian, W. Q.; West, D.; Sun, H.-B.; Zhang, S. B. Determination of Formation and Ionization Energies of Charged Defects in Two-Dimensional Materials. *Phys. Rev. Lett.* **2015**, *114*, 196801.

(13) Sundararaman, R.; Ping, Y. First-Principles Electrostatic Potentials for Reliable Alignment at Interfaces and Defects. *J. Chem. Phys.* **2017**, *146*, 104109.

(14) Freysoldt, C.; Neugebauer, J. First-Principles Calculations for Charged Defects at Surfaces, Interfaces, and Two-Dimensional Materials in the Presence of Electric Fields. *Phys. Rev. B* **2018**, *97*, 205425.

(15) Krukau, A. V.; Vydrov, O. A.; Izmaylov, A. F.; Scuseria, G. E. Influence of the Exchange Screening Parameter on the Performance of Screened Hybrid Functionals. *J. Chem. Phys.* **2006**, *125*, 224106−224112.

(16) Berseneva, N.; Krasheninnikov, A. V.; Nieminen, R. M. Mechanisms of Postsynthesis Doping of Boron Nitride Nanostructures with Carbon from First-Principles Simulations. *Phys. Rev. Lett.* **2011**, *107*, No. 035501.

(17) Ahmadpour Monazam, M. R.; Ludacka, U.; Komsa, H.-P.; Kotakoski, J. Substitutional Si Impurities in Monolayer Hexagonal Boron Nitride. *Appl. Phys. Lett.* **2019**, *115*, No. 071604.

(18) Lyons, J. L.; Van de Walle, C. G. Computationally Predicted Energies and Properties of Defects in GaN. *npj Comput. Mater.* **2017**, *3*, 1−10.

(19) Mapasha, R. E.; Molepo, M. P.; Andrew, R. C.; Chetty, N. Defect Charge States in Si Doped Hexagonal Boron-Nitride Monolayer. *J. Phys.: Condens. Matter* **2016**, *28*, No. 055501.

(20) Hinuma, Y.; Grüneis, A.; Kresse, G.; Oba, F. Band Alignment of Semiconductors from Density-Functional Theory and Many-Body Perturbation Theory. *Phys. Rev. B* **2014**, *90*, 155405.

(21) Jin, C.; Lin, F.; Suenaga, K.; Iijima, S. Fabrication of a Freestanding Boron Nitride Single Layer and Its Defect Assignments. *Phys. Rev. Lett.* **2009**, *102*, 195505.

(22) Novoselov, K. S.; Jiang, D.; Schedin, F.; Booth, T. J.; Khotkevich, V. V.; Morozov, S. V.; Geim, A. K. Two-Dimensional Atomic Crystals. *Proc. Natl. Acad. Sci. U. S. A.* **2005**, *102*, 10451−10453.

(23) Tran, T. T.; Bray, K.; Ford, M. J.; Toth, M.; Aharonovich, I. Quantum Emission from Hexagonal Boron Nitride Monolayers. *Nat. Nanotechnol.* **2016**, *11*, 37−41.

(24) Tawfik, S. A.; Ali, S.; Fronzi, M.; Kianinia, M.; Tran, T. T.; Stampfl, C.; Aharonovich, I.; Toth, M.; Ford, M. J. First-Principles Investigation of Quantum Emission from hBN Defects. *Nanoscale* **2017**, *9*, 13575−13582.

(25) Abdi, M.; Hwang, M.-J.; Aghtar, M.; Plenio, M. B. Spin-Mechanical Scheme with Color Centers in Hexagonal Boron Nitride Membranes. *Phys. Rev. Lett.* **2017**, *119*, 233602.
(26) Sajid, A.; Reimers, J. R.; Ford, M. J. Defect States in Hexagonal Boron Nitride: Assignments of Observed Properties and Prediction of Properties Relevant to Quantum Computation. *Phys. Rev. B* **2018**, *97*, No. 064101.
(27) Abdi, M.; Chou, J.-P.; Gali, A.; Plenio, M. B. Color Centers in Hexagonal Boron Nitride Monolayers: A Group Theory and Ab Initio Analysis. *ACS Photonics* **2018**, *5*, 1967−1976.
(28) Ivády, V.; Barcza, G.; Thiering, G.; Li, S.; Hamdi, H.; Legeza, Ö.; Chou, J.-P.; Gali, A. *Ab Initio Theory of Negatively Charged Boron Vacancy Qubit in h-BN*. 2019, ArXiv Prepr. ArXiv1910.07767. https://arxiv.org/abs/1910.07767.
(29) Ali, S.; Ford, M. J.; Reimers, J. R. Single-Photon Emitters in Hexagonal Boron Nitride: A Review of Progress. *Rep. Prog. Phys.* **2019**, DOI: 10.1088/1361-6633/ab6310.
(30) Gai, Y.; Tang, G. First-Principles Study of Native and Extrinsic Point Defects in Cubic Boron Nitride. *Phys. Scr.* **2011**, *83*, No. 045605.
(31) Wang, V.; Ma, N.; Mizuseki, H.; Kawazoe, Y. First-Principles Study of Intrinsic Defect Properties in Hexagonal BN Bilayer and Monolayer. *Solid State Commun.* **2012**, *152*, 816−820.
(32) Huang, B.; Lee, H. Defect and Impurity Properties of Hexagonal Boron Nitride: A First-Principles Calculation. *Phys. Rev. B* **2012**, *86*, 245406.
(33) Azevedo, S.; Kaschny, J. R.; de Castilho, C. M. C.; Mota, F. D. B. Corrigendum: Theoretical Investigation of Native Defects in a Boron Nitride Monolayer. *Nanotechnol.* **2012**, *23*, 489501.
(34) Zhang, Z.; Geng, Z.; Cai, D.; Pan, T.; Chen, Y.; Dong, L.; Zhou, T. Structure, Electronic and Magnetic Properties of Hexagonal Boron Nitride Sheets Doped by 5d Transition Metal Atoms: First-Principles Calculations and Molecular Orbital Analysis. *Phys. E* **2015**, *65*, 24−29.
(35) Attaccalite, C.; Bockstedte, M.; Marini, A.; Rubio, A.; Wirtz, L. Coupling of Excitons and Defect States in Boron-Nitride Nanostructures. *Phys. Rev. B* **2011**, *83*, 144115.
(36) Orellana, W.; Chacham, H. Stability of Native Defects in Hexagonal and Cubic Boron Nitride. *Phys. Rev. B* **2001**, *63*, 125205.
(37) Weston, L.; Wickramaratne, D.; Mackoit, M.; Alkauskas, A.; Van de Walle, C. G. Native Point Defects and Impurities in Hexagonal Boron Nitride. *Phys. Rev. B* **2018**, *97*, 214104.
(38) Turiansky, M. E.; Alkauskas, A.; Bassett, L. C.; Van de Walle, C. G. Dangling Bonds in Hexagonal Boron Nitride as Single-Photon Emitters. *Phys. Rev. Lett.* **2019**, *123*, 127401.
(39) Perdew, J. P.; Burke, K.; Ernzerhof, M. Generalized Gradient Approximation Made Simple. *Phys. Rev. Lett.* **1996**, *77*, 3865−3868.
(40) Blöchl, P. E. Projector Augmented-Wave Method. *Phys. Rev. B* **1994**, *50*, 17953−17979.
(41) Kresse, G.; Furthmüller, J. Efficient Iterative Schemes for Ab *Initio* Total-Energy Calculations Using a Plane-Wave Basis Set. *Phys. Rev. B* **1996**, *54*, 11169−11186.
(42) Wang, V.; Xu, N.; Liu, J.-C.; Tang, G.; Geng, W.-T. *Vaspkit: A Pre- and Post-Processing Program for Vasp Code*. 2019, ArXiv Prepr. ArXiv190808269. https://arxiv.org/abs/1908.08269.
(43) Naik, M. H.; Jain, M. Coffee: Corrections for Formation Energy and Eigenvalues for Charged Defect Simulations. *Comput. Phys. Commun.* **2018**, *226*, 114−126.
(44) Shirodkar, S. N.; Waghmare, U. V.; Fisher, T. S.; Grau-Crespo, R. Engineering the Electronic Bandgaps and Band Edge Positions in Carbon-Substituted 2D Boron Nitride: A First-Principles Investigation. *Phys. Chem. Chem. Phys.* **2015**, *17*, 13547−13552.
(45) Noh, J.-Y.; Kim, H.; Kim, Y.-S. Stability and Electronic Structures of Native Defects in Single-Layer MoS_2. *Phys. Rev. B* **2014**, *89*, 205417.

https://dx.doi.org/10.1021/acsami.9b23431
ACS Appl. Mater. Interfaces 2020, 12, 17055−17061